

Temporally-Extended Prompts Optimization for SAM in Interactive Medical Image Segmentation

Chuyun Shen

*School of Computer Science and Technology
East China Normal University
Shanghai 200062, China*

CYSHEN@STU.ECNU.EDU.CN

Wenhao Li

*School of Data Science
The Chinese University of Hong Kong, Shenzhen
Shenzhen Institute of Artificial Intelligence and Robotics for Society
Shenzhen 518172, China*

LIWENHAO@CUHK.EDU.CN

Ya Zhang

*Cooperative Medianet Innovation Center
Shanghai Jiao Tong University
Shanghai, 200240, China*

YA_ZHANG@SJTU.EDU.CN

Xiangfeng Wang

*School of Computer Science and Technology
East China Normal University
Shanghai 200062, China*

XFWANG@CS.ECNU.EDU.CN

Abstract

The *Segmentation Anything Model* (SAM) has recently emerged as a foundation model for addressing image segmentation. Owing to the intrinsic complexity of medical images and the high annotation cost, the medical image segmentation (MIS) community has been encouraged to investigate SAM’s zero-shot capabilities to facilitate automatic annotation. Inspired by the extraordinary accomplishments of *interactive* medical image segmentation (IMIS) paradigm, this paper focuses on assessing the potential of SAM’s zero-shot capabilities within the IMIS paradigm to amplify its benefits in the MIS domain. Regrettably, we observe that SAM’s vulnerability to prompt forms (e.g., points, bounding boxes) becomes notably pronounced in IMIS. This leads us to develop a framework that adaptively offers suitable prompt forms for human experts. We refer to the framework above as *temporally-extended prompts optimization* (TEPO) and model it as a Markov decision process, solvable through reinforcement learning. Numerical experiments on the standardized benchmark BraTS2020 demonstrate that the learned TEPO agent can further enhance SAM’s zero-shot capability in the MIS context.

1. Introduction

The *Segmentation Anything Model* (SAM) (Kirillov et al., 2023) has recently been proposed as a foundational model for addressing image segmentation problems. SAM’s effectiveness is principally evaluated in natural image domains, demonstrating a remarkable prompt-based, zero-shot generalization capability. Segmentation within medical images (MIS), on the other hand, presents complex challenges owing to their substantial deviation from natural images,

encompassing multifaceted modalities, intricate anatomical structures, indeterminate and sophisticated object boundaries, and extensive object scales (Sharma and Aggarwal, 2010; Hesamian et al., 2019; Huang et al., 2023).

Predominant MIS methods principally employ domain-specific architectures and necessitate reliance upon massive, high-quality expert annotations (Ronneberger et al., 2015; Isensee et al., 2021; Zhou et al., 2021; Cao et al., 2023). In light of the considerable expenditure incurred by dense labeling, the community has embarked on exploring SAM’s zero-shot generalization capabilities in MIS tasks, thereby fostering automated annotation of medical images (Ji et al., 2023a,b; Mohapatra et al., 2023; Deng et al., 2023; Zhou et al., 2023; He et al., 2023; Mazurowski et al., 2023; Ma and Wang, 2023; Cheng et al., 2023; Zhang and Jiao, 2023; Roy et al., 2023; Huang et al., 2023; Mattjie et al., 2023).

Motivated by the remarkable achievements of *interactive* medical image segmentation (IMIS), this paper goes a step further and centers on investigating the potential of zero-shot capabilities of SAM in the IMIS domain to magnify the advantages of SAM in MIS domain. An extensive body of research demonstrates the significant performance enhancement attributable to the IMIS paradigm (Xu et al., 2016; Rajchl et al., 2016; Lin et al., 2016; Castrejon et al., 2017; Wang et al., 2018; Song et al., 2018; Liao et al., 2020; Ma et al., 2021; Li et al., 2021). Specifically, IMIS overcomes the performance limitation inherent in end-to-end MIS approaches by reconceptualizing MIS as a multi-stage, human-in-the-loop task. At each iterative stage, medical professionals impart valuable feedback (e.g., designating critical points, demarcating boundaries, or construing bounding boxes) to identify inaccuracies in the model output. Consequently, the model refines the segmentation results following expert knowledge embedded in human feedback.

The congruity between the human feedback forms in IMIS and the prompt forms in SAM facilitates the seamless integration of SAM within the IMIS framework. Nevertheless, recent investigations reveal that, in contrast to natural image segmentation, the susceptibility of the SAM model to prompt forms (e.g., points or bounding boxes) is significantly heightened within MIS tasks, resulting in substantial discrepancies in zero-shot performance when various prompt forms are employed (Cheng et al., 2023; Roy et al., 2023; Zhang and Jiao, 2023). Regrettably, we find this issue is markedly exacerbated within the IMIS context.

This phenomenon can be attributed to two primary factors. Firstly, the segmentation stages are interdependent; the previous prompt forms selection directly impacts the ensuing segmentation, which, in turn, influences the choice of subsequent prompt forms. Secondly, human experts display preferences and stochasticity in their feedback, seldom contemplating the ramifications of the prompt forms on the performance and the intricate interconnections between antecedent and successive prompt forms. Consequently, this revelation impels us to recommend the most efficacious prompt forms for human feedback at each successive IMIS stage, a challenge we designate as *temporally-extended prompts optimization*.

As a formidable instrument for addressing sequential decision-making, reinforcement learning (RL) (Sutton and Barto, 2018) demonstrates remarkable competencies not only in domains such as chess, video games, and robotics control but also in training foundational models (Ouyang et al., 2022; Wei et al., 2022) and IMIS (Liao et al., 2020; Ma et al., 2021; Li et al., 2021). Given that temporally-extended prompt optimization encompasses both the foundational model and IMIS, we formulate this problem as a Markov decision process (MDP) and employ RL for its resolution. The framework above is then instantiated as the

algorithm denoted by **TEPO**. During each stage, TEPO agent determines which prompt form is most suitable for recommendation to human, considering the current segmentation outcomes and historical prompts. The ultimate objective is to augment the performance of the SAM in each stage relative to its preceding iteration, thereby maximizing its efficacy.

The contributions presented in this paper encompass three distinct aspects: 1) In an unprecedented discovery, we ascertain that sequential prompt forms constitute the crucial elements influencing the zero-shot performance of SAM in IMIS, subsequently proposing a pertinent temporally-extended prompts optimization problem; 2) By conceptualizing the temporally-extended prompts optimization as an MDP, we employ RL to optimize the sequential selection of prompt forms, thereby enhancing the zero-shot performance of SAM in IMIS; 3) The performance juxtaposition and ablation studies conducted on the standardized benchmark BraTS2020 substantiate the efficacy of the TEPO agent in ameliorating SAM’s zero-shot capability.

2. Related Work and Preliminaries

2.1 Interactive Medical Image Segmentation

Before the remarkable advancements in automatic segmentation achieved through convolutional neural networks (CNNs), traditional interactive techniques were employed within IMIS (Zhao and Xie, 2013). Among these techniques, the RandomWalk method (Grady, 2006) generates a weight map with pixels as vertices and segments images based on user interaction. Approaches like GrabCut (Rother et al., 2004) and GraphCut (Boykov and Jolly, 2001) establish a connection between image segmentation and graph theory’s maximum flow and minimum cut algorithms. Geos (Criminisi et al., 2008) introduces a geodesic distance measurement to ascertain pixel similarity.

There has been a surge of interest in deep learning-based IMIS methods in recent years. Xu et al. (2016) suggests employing CNNs for interactive image segmentation, whereas DeepCut (Rajchl et al., 2016) and ScribbleSup (Lin et al., 2016) utilize weak supervision in developing interactive segmentation techniques. DeepIGeoS (Wang et al., 2018) incorporates a geodesic distance metric to generate a hint map.

The interactive segmentation process can be viewed as a sequential procedure, which makes it a natural fit for reinforcement learning (RL). Polygon-RNN (Castrejon et al., 2017) tackles this problem by segmenting targets as polygons and iteratively selecting polygon vertices through a recurrent neural network (RNN). With a similar approach, Polygon-RNN+ (Acuna et al., 2018) adopts a similar approach to Polygon-RNN, it employs RL to learn vertex selection. SeedNet (Song et al., 2018) takes a different approach by constructing an expert interaction generation RL model that can obtain simulated interaction data at each interaction stage.

IteR-MRL (Liao et al., 2020) and BS-IRIS (Ma et al., 2021) conceptualize the dynamic interaction process as a Markov Decision Process (MDP) and apply multi-agent RL models for image segmentation purposes. MECCA (Li et al., 2021), based on IteR-MRL, establishes a confidence network, seeking to mitigate the pervasive “interactive misunderstanding” issue that plagues RL-based IMIS techniques and ensure the effective utilization of human feedback. Additionally, Liu et al. (2023) integrates the SAM within the *3D Slicer* software, thereby facilitating the process of designing, evaluating, and employing SAM in the context of IMIS.

2.2 Segment Anything Model

The *Segmentation Anything Model* (SAM) (Kirillov et al., 2023), recently introduced by Meta, serves as a fundamental framework for tackling image segmentation challenges. Motivated by the robust performance of foundational models in NLP and CV domains, researchers endeavored to establish a unified model for complete image segmentation tasks. Nonetheless, the actual data in the segmentation field necessitates revision and diverges from the design intentions mentioned above. Consequently, Kirillov et al. (2023) stratifies the process into three distinct phases: *task*, *model*, and *data*. Refer to the primary publication (Kirillov et al., 2023) and a contemporary survey (Zhang et al., 2023) for comprehensive explanations.

Task. Drawing inspiration from foundational NLP and CV models, Kirillov et al. (2023) introduces the promptable segmentation task to generate a valid segmentation mask in response to any given segmentation prompt. These prompts define the target object(s) to be segmented within an image and may include a location point, a bounding box, or a textual description of the object(s). The resulting mask must be plausible for at least one target object, even in instances where the prompt may be ambiguous or reference multiple objects.

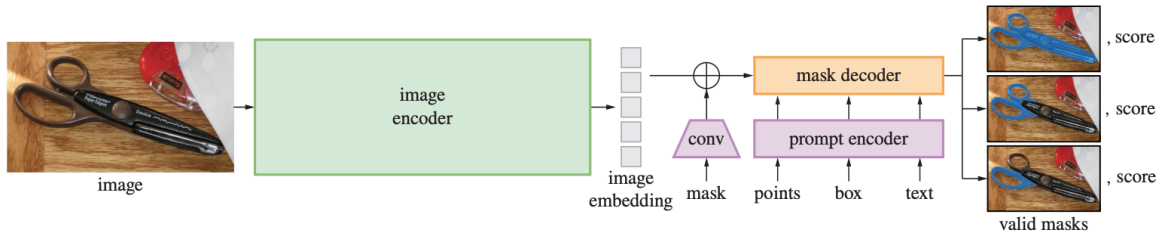


Figure 1: The screenshot of SAM (Kirillov et al., 2023).

Model. The promptable segmentation task, paired with the objective of real-world applicability, imposes restrictions on the model architecture. Kirillov et al. (2023) devises a streamlined yet efficacious model, known as SAM (Figure 1), which encompasses a powerful image encoder that computes image embeddings, a prompt encoder that embeds prompts, and a lightweight mask decoder that amalgamates the two information sources to predict segmentation masks.

Data. SAM necessitates training on an extensive and diverse collection of masks to attain exceptional generalization capabilities on novel data distributions. Kirillov et al. (2023) constructs a "data engine", employing a model-in-the-loop dataset annotation approach, thereby co-developing SAM in tandem. The resulting dataset, SA-1B, incorporates over 1 billion masks derived from 11 million licensed and privacy-preserving images.

2.3 Segment Anything in Medical Images

Building upon the foundational pre-trained models of SAM, many papers have delved into investigating its efficacy in diverse zero-shot MIS scenarios. Ji et al. (2023a) conducts a comprehensive evaluation of SAM in the *everything* mode for segmenting lesion regions within an array of anatomical structures (e.g., brain, lung, and liver) and imaging modalities (*computerized tomography*, abbreviated as CT, and *magnetic resonance imaging*, abbreviated as MRI). Ji et al. (2023b) subsequently scrutinizes SAM's performance in specific healthcare

domains (optical disc and cup, polyp, and skin lesion segmentation) utilizing both the automatic *everything* mode and the manual *prompt* mode, employing points and bounding boxes as prompts.

For MRI brain extraction tasks, Mohapatra et al. (2023) compares SAM’s performance with the renowned *Brain Extraction Tool* (BET), a component of the *FMRIB Software Library*. Deng et al. (2023) appraises SAM’s performance in digital pathology segmentation tasks, encompassing tumor, non-tumor tissue, and cell nuclei segmentation on high-resolution whole-slide imaging. Zhou et al. (2023) adeptly implements SAM in polyp segmentation tasks, utilizing 5 benchmark datasets under the *everything* setting. Recently, an assortment of studies has rigorously tested SAM on over 10 publicly available MIS datasets or tasks (He et al., 2023; Mazurowski et al., 2023; Ma and Wang, 2023; Wu et al., 2023; Huang et al., 2023; Zhang and Liu, 2023).

Quantitative experimental results gleaned from these works reveal that the zero-shot performance of SAM is, on the whole, moderate and exhibits variability across distinct datasets and cases. To elaborate: 1) Utilizing *prompt* instead of *everything* mode, SAM can surpass state-of-the-art (SOTA) performance in tasks characterized by voluminous objects, smaller quantities, and well-defined boundaries when reliant on dense human feedback; 2) However, a considerable performance discrepancy remains between SAM and SOTA methods in tasks involving dense and amorphous object segmentation.

3. Temporally-extended Prompts Optimization Methodology

As elucidated in the preceding analysis, the susceptibility of SAM to prompt forms is markedly pronounced in IMIS. This serves as the impetus for devising a framework adept at adaptively proffering suitable prompt forms for human specialists, contingent upon the current progression of segmentation. The human expert subsequently imparts feedback to SAM, employing the recommended prompt form. The ensuing discourse delineates the modeling of this framework, the temporally-extended prompts optimization, as an MDP (Section 3.1) and elaborates on its solution through reinforcement learning (Section 3.2).

3.1 Problem Formulation

We consider a standard setup consisting of an agent interacting with an environment in discrete timesteps. In our setting, the purpose of the agent is to recommend appropriate prompt forms for human experts. At each timestep t the agent receives an observation o_t , takes an action a_t and receives a scalar reward r_t . In general, the environment may be partially observed so that the entire history of the observations, action pairs $s_t = (o_1, a_1, \dots, a_{t-1}, o_t)$ may be required to describe the state.

The behavior of an agent is defined by a policy, π , which maps states to a probability distribution over actions $\pi : \mathcal{S} \rightarrow \mathcal{P}(\mathcal{A})$. We model it as a Markov decision process with state space \mathcal{S} , action space \mathcal{A} , initial state distribution $p(s_1)$, transition dynamics $p(s_{t+1} | s_t, a_t)$, reward function $r(s_t, a_t)$, and instantiate it as follows:

State space. The state at timestep t is represented as a three-tuple $S_t = (I, P_{t-1}, T_{t-1})$, where $I \in \mathbb{R}^{H \times W \times C}$ represents the medical image slice input, $P_{t-1} \in \mathbb{R}^{H \times W \times K}$ represents the segmentation logits from the previous time step $t - 1$ (where K represents the number

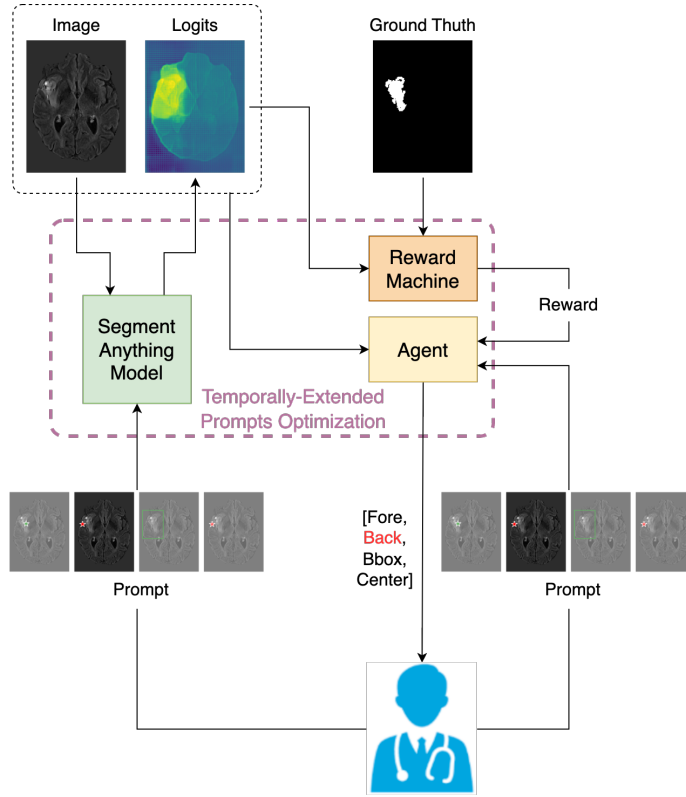


Figure 2: The architecture of our proposed TEPO.

of segmentation classes, which in this case is 2), and T_{t-1} is a set of interaction prompts provided before time step t . We consider four types of interaction prompts form at each timestep: forehead, background, center point, and bounding box, and we will introduce them in Section 4.2.

Action space. The action space \mathcal{A} is a set of interactive forms provided by human experts at each time step. It is represented as a set of integers $\mathcal{A} = \{0, 1, 2, 3\}$, where 0 denotes selecting the forehead point, 1 denotes accessing the background point, 2 denotes the center point, which is defined as the point farthest from the boundary of the error regions, and 3 denotes selecting the bounding box. At each time step, the agent chooses an action from the action space \mathcal{A} to assist human experts with their interactions with SAM.

Reward function. At each step t , the difference between the current DICE score (Dice, 1945), $dice(P_t, Y)$ and the previous DICE score, $dice(P_{t-1}, Y)$, is calculated as the reward value R_t :

$$R_t = dice(P_t, Y) - dice(P_{t-1}, Y),$$

where Y is the ground truth, $dice(P_t, Y)$ represents the DICE score between the current predicted result P_t and the ground truth, and $dice(P_{t-1}, Y)$ represents the DICE score between the previous predicted result and the ground truth.

In summary, as shown in Figure 2, the whole process is as follows: the agent gives the recommended prompt form in accordance with the policy π based on the raw image, the

current segmentation probability and the hints given by the doctor. Then the doctor gives the SAM the corresponding prompt and updates the segmentation probability. The changes in the segmentation result are used by the agent as the reward to update the policy π .

In addition, the *return* from a state is defined as the sum of discounted future reward $R_t = \sum_{i=t}^T \gamma^{(i-t)} r(s_i, a_i)$ with a discounting factor $\gamma \in [0, 1]$. Depending on this problem formulation, the goal of temporally-extended prompts optimization is to learn a policy that maximizes the expected return from the start distribution $J = \mathbb{E}_{r_i, s_i \sim E, a_i \sim \rho^\pi} [R_1]$. We denote the discounted state visitation distribution for a policy π as ρ^π .

3.2 Learning the TEPO Agent with RL

Before introducing RL methods to obtain the optimal prompt, we first introduce some notations. The *action-value function* is used in many RL algorithms. It describes the expected return after taking an action a_t in state s_t and thereafter following policy π :

$$Q^\pi(s_t, a_t) = \mathbb{E}_{r_{i \geq t}, s_{i > t} \sim E, a_{i > t} \sim \pi} [R_t | s_t, a_t]. \quad (1)$$

Additionally, many approaches in RL make use of the recursive relationship known as the *Bellman equation*:

$$Q^\pi(s_t, a_t) = \mathbb{E}_{r_t, s_{t+1} \sim E} [r(s_t, a_t) + \gamma \mathbb{E}_{a_{t+1} \sim \pi} [Q^\pi(s_{t+1}, a_{t+1})]]. \quad (2)$$

This paper adopts deep Q -network (DQN) (Mnih et al., 2013, 2015) to instantiate the RL framework and learn the TEPO agent. Q -learning (Watkins and Dayan, 1992), as the core module of DQN, is a commonly-used, off-policy RL algorithm, by employing the greedy policy $\mu(s) = \arg \max_a Q(s, a)$. DQN adapts the Q -learning to make effective use of large neural networks as action-value function approximators. We consider function approximators parameterized by θ^Q , which we optimize by minimizing the loss:

$$\mathcal{L}(\theta^Q) = \mathbb{E}_{s_t \sim \rho^\beta, a_t \sim \beta, r_t \sim E} [(Q(s_t, a_t | \theta^Q) - y_t)^2], \quad (3)$$

where $y_t = r(s_t, a_t) + \gamma Q(s_{t+1}, \mu(s_{t+1}) | \theta^Q)$. The full algorithm, which we call TEPO, is presented in Algorithm 1.

4. Experiments on MIS

This section provides an evaluation of the proposed TEPO on the BraTS2020 benchmark, which is a prevalent dataset used for MIS tasks. We aim to address the following key questions, and the following evaluation will focus on answering these questions comprehensively, i.e.,

- a) Does the SAM with multi-step interaction outperform the SAM with single-step interaction?
- b) Can the policies learned by the TEPO algorithm outperform the rule-based policies?
- c) What strategies can be learned from TEPO?
- d) How stable are the strategies learned by TEPO?

4.1 Dataset and Training Details

SAM requires 2D images as input and 3D images are conventionally often annotated by viewing them in slices, we adopt the practice of slicing the 3D magnetic resonance scans into axial slices, a method commonly used in related research efforts (Wolleb et al., 2022).

Algorithm 1: Temporally-Extended Prompts Optimization

```

1 Initialize replay memory  $\mathcal{D}$  to capacity  $N$ 
2 Initialize action-value function  $Q$  with random weights
3 for  $episode = 1, M$  do
4   Randomly sample an image  $I$ , and encode it with SAM
5   Initialise state  $s_1 = (I, P_0, T_0)$ , where  $P_0 = \mathbf{0}$  and  $T_0 = \emptyset$ 
6   for  $t = 1, T$  do
7     With probability  $\epsilon$  select a random avail interaction form  $a_t$ ; otherwise select
        $a_t = \max_a Q^*(s_t, a; \theta)$ 
8     Execute action  $a_t$  and doctor make a prompt based on  $a_t$  and  $s_t$ , and then
       SAM input prompts  $T_t$  and update logit  $P_t$ 
9     Reward  $r_t = r(s_t, a_t)$  and update state  $s_{t+1} = (I, P_t, T_t)$ 
10    Store transition  $(s_t, a_t, r_t, s_{t+1})$  in  $\mathcal{D}$ 
11    Sample random minibatch of transitions  $(s_j, a_j, r_j, s_{j+1})$  from  $\mathcal{D}$ 
12    Set greedy action  $\mu(s) = \arg \max_a Q(s, a)$ 
13    Set  $y_j = \begin{cases} r_j & \text{for terminal } s_{j+1} \\ r_j + \gamma Q(s_{j+1}, \mu(s_{j+1}) | \theta^Q) & \text{for non-terminal } s_{j+1} \end{cases}$ 
14    Perform gradient descent based on the Bellman error  $(Q(s_t, a_t | \theta^Q) - y_t)^2$ 
15  end for
16 end for

```

To evaluate the effectiveness of TEPO in the context of multi-step interaction, we carefully selected slices with sufficiently large foregrounds in the image. Specifically, we segment the *Whole Tumor* (WT) from the *FLAIR* images and choose slices that contain a minimum of 256 foreground pixel points for analysis. This carefully curated dataset enables accurate evaluation of the performance and potential of TEPO in future applications in MIS.

The dataset for evaluation comprised a total of 369 patients. We split the dataset into three subsets: the training set evaluated 319 patients and included 17,396 slices; the validation set consisted of 20 patients, corresponding to 1,450 slices; and the test set included 20 patients with 1,389 slices.

We crop the images to 200×150 , implement *random flip, rotate, add noise, affine transform* data augmentation to the training dataset, and then rescale the intensity values. We train for 100 epochs, and in each epoch, 10,000 steps are sampled, and the Q network of TEPO is updated 100 times. The model is trained with a learning rate of $1e^{-3}$ for the **Adam** optimizer and a batch size of 64.

4.2 Main Results

The performance of the proposed TEPO algorithm is evaluated on the BraTS2020 dataset for medical image segmentation tasks and compared with three rule-based policy baselines: the one-step oracle agent, the random agent, and the alternately changing agent. The one-step oracle agent is an optimal decision-making agent that has access to comprehensive information and can observe the reward after adapting various interaction forms. This allows it to achieve the highest accuracy in a single step and to explore efficient interaction strategies

Table 1: Action selection preference statistics and quantitative segmentation performance results for TEPO policies and rule-based policies. Labels used in the paper include “Fore” for the forehead point form, “Back” for the background point form, “Center” for the center point form, and “Bbox” for the bounding box form. These labels will be consistently used throughout the paper. “<-0.1” indicates the number of cases that reward less than 0.1, which means the algorithm misunderstands the interaction. In addition, we use boldface to indicate the highest dice score in each step.

Algorithm	variable	Step 1	Step 2	Step 3	Step 4	Step 5	Step 6	Step 7	Step 8	Step 9
TEPO-2	Action	Bbox (100.00%)	Fore (99.57%)	Fore (99.78%)	Fore (99.71%)	Fore (99.86%)	Fore (99.86%)	Fore (99.86%)	Fore (99.86%)	Fore (99.93%)
	Dice	0.6901± 0.2094	0.6930± 0.1758	0.6937± 0.1694	0.6932± 0.1692	0.6940± 0.1693	0.6940± 0.1693	0.6940± 0.1694	0.6940± 0.1694	0.6940± 0.1694
	-0.1	0	95	14	2	0	0	0	0	0
TEPO-3	Action	Center (100.00%)	Bbox (94.96%)	Center (98.85%)	Center (99.14%)	Center (99.78%)	Center (100.00%)	Center (99.86%)	Center (100.00%)	Center (100.00%)
	Dice	0.4658± 0.2877	0.7035± 0.1882	0.7611± 0.1687	0.7845± 0.1670	0.8026± 0.1553	0.8198± 0.1441	0.8263± 0.1409	0.8332± 0.1367	0.8362± 0.1378
	-0.1	0	54	44	72	73	46	47	45	44
TEPO-5	Action	Center (100.00%)	Center (62.35%)	Center (86.54%)	Center (95.10%)	Center (97.48%)	Center (99.57%)	Center (99.64%)	Center (99.71%)	Center (99.64%)
	Dice	0.4658± 0.2877	0.6472± 0.2316	0.7369± 0.1926	0.7782± 0.1665	0.8021± 0.1577	0.8190± 0.1439	0.8288± 0.1375	0.8372± 0.1346	0.8421± 0.1322
	-0.1	0	117	102	103	85	62	48	44	42
TEPO-7	Action	Center (100.00%)	Bbox (85.67%)	Center (79.34%)	Center (90.78%)	Center (93.38%)	Center (94.89%)	Center (95.39%)	Center (95.82%)	Center (95.61%)
	Dice	0.4658± 0.2877	0.6981± 0.1965	0.7552± 0.1720	0.7822± 0.1690	0.7991± 0.1612	0.8137± 0.1520	0.8240± 0.1424	0.8316± 0.1370	0.8342± 0.1380
	-0.1	0	56	56	65	62	53	40	45	41
TEPO-9	Action	Center (100.00%)	Center (100.00%)	Center (100.00%)	Center (100.00%)	Center (100.00%)	Center (100.00%)	Center (100.00%)	Center (100.00%)	Center (100.00%)
	Dice	0.4658± 0.2877	0.6211± 0.2535	0.7192± 0.2131	0.7707± 0.1711	0.7990± 0.1583	0.8175± 0.1452	0.8302± 0.1390	0.8394± 0.1324	0.8449± 0.1307
	-0.1	0	177	153	167	123	86	58	51	51
Random	Action	Center (26.78%)	Center (29.30%)	Fore (30.67%)	Fore (33.48%)	Back (32.04%)	Fore (33.48%)	Center (33.33%)	Back (33.33%)	Fore (33.55%)
	Dice	0.4129 ± 0.3417	0.5723 ± 0.2947	0.6561 ± 0.2562	0.7072 ± 0.2260	0.7354 ± 0.2094	0.7571 ± 0.1943	0.7818 ± 0.1727	0.7956 ± 0.1627	0.8052 ± 0.1568
	-0.1	0	121	141	123	115	89	66	50	39
Alternately	Action	Fore (100.00%)	Back (100.00%)	Fore (100.00%)	Back (100.00%)	Fore (100.00%)	Back (100.00%)	Fore (100.00%)	Back (100.00%)	Fore (100.00%)
	Dice	0.4658 ± 0.2877	0.6010 ± 0.2691	0.6460 ± 0.2470	0.7280 ± 0.2067	0.7332 ± 0.2098	0.7823 ± 0.1730	0.7840 ± 0.1777	0.8138 ± 0.1512	0.8052 ± 0.1652
	-0.1	0	98	207	98	172	59	111	27	92

for the given task. The random agent, on the other hand, uniformly samples actions from available action sets and can be used to simulate clinicians without any preference for any particular interaction form for the task at hand. The alternately changing agent applies a policy that alternately chooses the forehead point and the background point.

We evaluate the agent’s performance through the dice score, computed using a ground truth mask and measurements taken at multiple timesteps ($N = \{2, 3, 5, 7, 9\}$). At each timestep, the agent first chooses an action to indicate what form of interaction is required. To simulate a clinician’s behavior, we use rules consisting of choosing specific positions, such as the forehead, background, and center, and drawing bounding boxes around the forehead region. Specifically, we select the forehead, background, and center points that are farthest from the boundaries of the false negative, false positive, and error regions, respectively. For the bounding box, we extend the forehead region by 10 pixels and draw a rectangle.

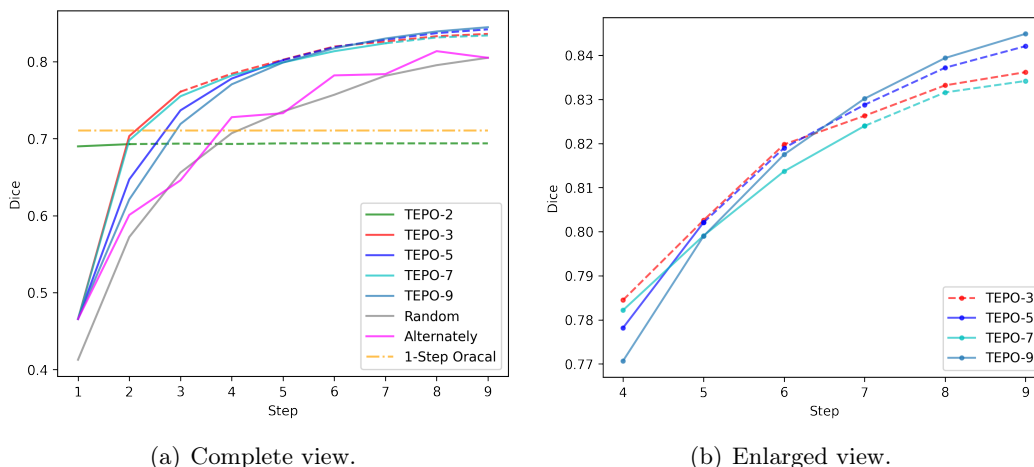


Figure 3: The performance improvement of different IMIS methods at different interaction steps. All these test results are performed on the BraTS2020 dataset. Subfigure (a) illustrate various IMIS methods from step one to step nine. To compare the performances of the algorithms, Subfigure (b) shows an enlarged view of steps four to nine, only including those with dice scores larger than 0.75.

The comparison of the performance of various interaction strategies is evaluated with respect to the number of interactions. As shown in Figure 3, the different lines correspond to the different agents’ performance. “TEPO- X ” indicates that the agent is trained in the X -step interaction scenario. For example, “TEPO-2” means a two-step scenario. “Random” denotes the random agent, “Alternately” denotes the alternately changing agent, and “1-step Oracal” denotes the one-step Oracal agent. We will use the same labeling convention throughout the paper unless noted otherwise. It is worth noting that we train in different interaction step scenarios, but in testing, we use 9-step interactions to find out comprehensive performances.

4.2.1 QUANTITATIVE EXPERIMENTAL ANALYSIS

Q#a: Does the SAM in multi-step interaction mode outperform the SAM in single-step interaction mode? As illustrated in Figure 3, the TEPO-2 agent stays the

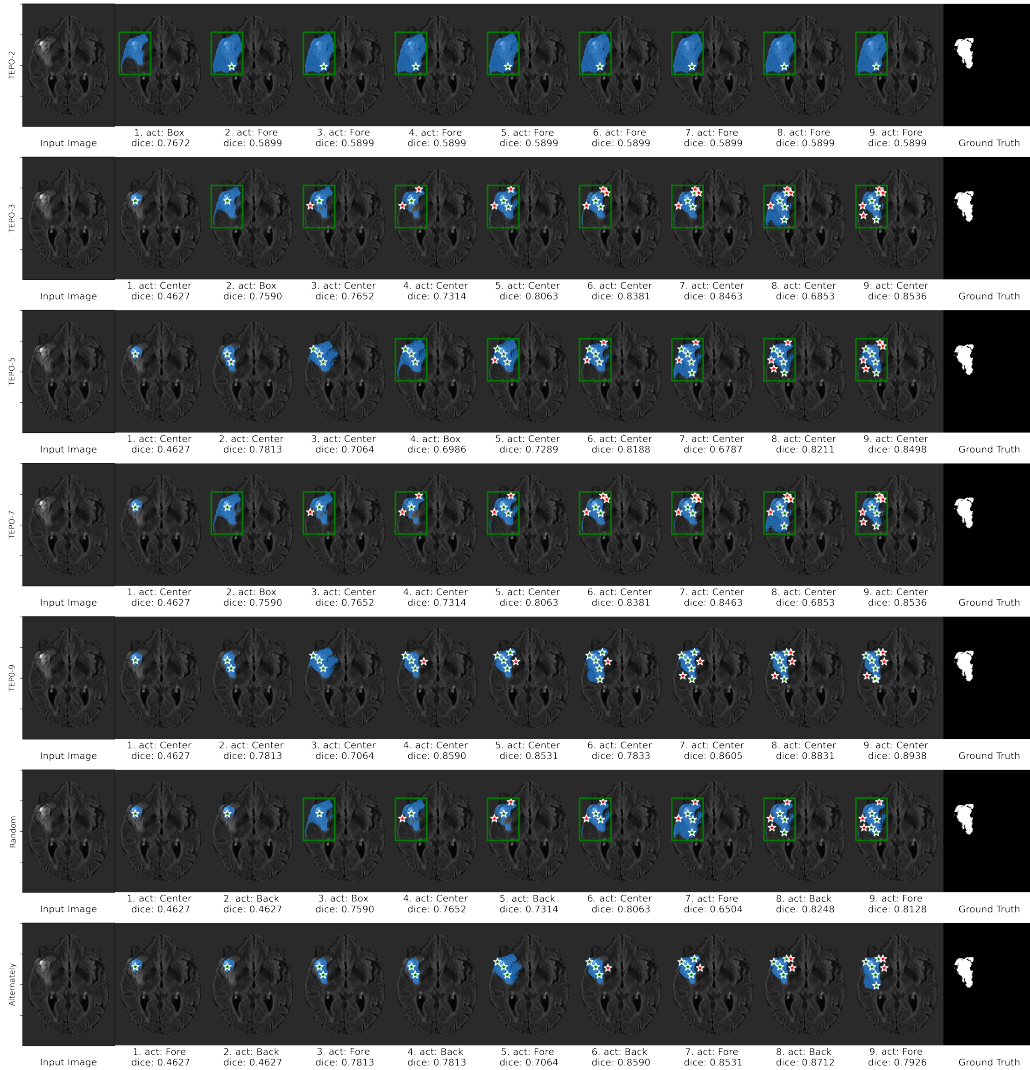


Figure 4: Visualization of strategies and results of different strategies on the same medical image. The green pentagram indicates the foreground, the red pentagram indicates the background, and the green box indicates the bounding box.

same after the third round, this is because in our experiments, if the shortest distance of all points from the edge in the corresponding region is less than two pixels, then the user does not interact anymore. Table 1 indicates that the TEPO-2 policy predominantly selects the forehead point starting from step two. However, the false negative region is too small to click, so the TEPO-2 policy stops interacting at step five for all test cases. Conversely, the performance of other multi-step policies improves with an increase in the number of interactions, showcasing that SAM can be enhanced through multiple rounds of interactions. Moreover, expect TEPO-2, other policies perform better than the one-step Oracle agent, implying that multi-step interactions are more effective for medical image segmentation than the single-step interaction mode.

Q#b: Can the policies learned by the TEPO algorithm outperform the rule-based policies? The experimental results in Figure 3 indicate that the TEPO-2 policy performs better than random and alternating selection methods during the initial two interactions. Moreover, the performance of all other RL-based policies is superior to rule-based approaches. These findings provide evidence that the TEPO algorithm significantly boosts the efficacy of SAM in interactive medical scenarios, even in zero-shot mode.

Q#c: What strategies can be learned from the TEPO algorithm? As the TEPO algorithm is trained under different interaction round scenarios, the learned strategies exhibit variations, as summarized in Table 1. TEPO-2 employs a straightforward strategy: selecting the bounding box in the first step and the forehead point in subsequent ones. This strategy performs well in the initial two steps, with the performance in the first step nearing that of the one-step Oracle agent that adopts an ideal strategy. TEPO-3 applies a nearly deterministic strategy that chooses the bounding box at the second step and chooses center points at other steps. Moreover, TEPO-5 and TEPO-7 use more uncertain strategies that primarily employ the center point but may resort to alternative ones in the second and third steps. TEPO-9 finds a trivial strategy of choosing the center point at each step, resulting in the best performance in multiple interactions.

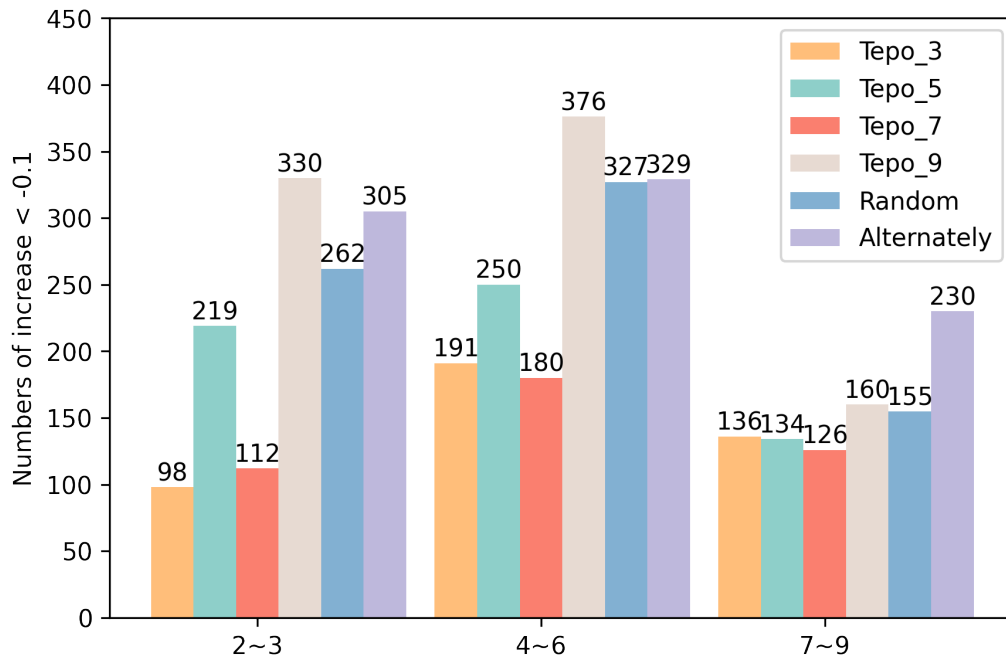


Figure 5: Comparison of the number of cases with increased dice score less than -0.1 .

Q#d: How stable are the strategies learned by TEPO? One issue that may affect the performance of TEPO is interactive misunderstanding, where user interactions result in reduced segmentation dice scores. In this study, we consider interactive misunderstandings when the segmentation dice score decreases by over 0.1. We analyze the occurrence of interactive misunderstandings for different strategies on our test data, as presented in Tables

1. For a more intuitive comparison, we plot the number of interactive misunderstandings for each strategy at different interaction steps in Figure 5. As TEPO-2 only applies to the initial two interactions, we exclude it from the plot. Resultantly, the findings indicate that TEPO-3, TEPO-5, and TEPO-7 exhibit fewer misunderstandings than the random and alternating agents, thereby indicating superior stability and performance.

4.2.2 QUALITATIVE EXPERIMENTAL ANALYSIS

To evaluate the effectiveness of different strategies and investigate the causes of misunderstandings that occur with SAM, we conducted a qualitative analysis and present their performance on a single medical image in Figure 4. The first column displays the raw image, while the middle columns show the interaction processes and corresponding segmentation outcomes. The last column provides the ground truth. Among the different strategies, TEPO-2 demonstrates relatively weak performance, as it only involves two effective interactions. The TEPO-9 and alternately changing agent purely used point-based interaction. TEPO-9 produces an equally good final outcome compared to the strategy with the bounding box and obtains the best result finally after nine interactions, the alternately changing policy performs poorly due to less effective interactions. TEPO-3, and TEPO-7 consistently use the bounding box in the second interaction and select center points in all other interactions. TEPO-5 uses the bounding box in the fourth interaction and center points in all other interactions. These three policies produce similar final results. In addition, we observe a misunderstanding issue in some interactions, such as the seventh interaction with TEPO-5, and the eighth interaction with TEPO-3 and TEPO-7. This is likely due to the corresponding region being too small for SAM to adequately understand the human feedback.

Overall, our results suggest that SAM cannot accurately achieve segmentation in a single interaction in medical tasks without being properly tuned. However, with multiple rounds of interaction, it can achieve considerable results. Moreover, the strategies learned by TEPO demonstrate better segmentation performance compared to rule-based strategies.

5. Conclusion

This paper focuses on assessing the potential of SAM’s zero-shot capabilities within the interactive medical image segmentation (IMIS) paradigm to amplify its benefits in the medical image segmentation (MIS) domain. We introduce an innovative reinforcement learning-based framework, *temporally-extended prompts optimization* (TEPO), to optimize prompts that can enhance segmentation accuracy in multi-step interaction situations. Our empirical study, conducted on the BraTS2020 benchmark, highlights the prompt sensitivity of SAM and demonstrates that TEPO can further enhance its zero-shot capability in the MIS domain. Specifically, TEPO successfully reduces the incidence of interactive misunderstandings, thus improving segmentation accuracy and stability in medical images. These findings make a valuable contribution to the development of advanced MIS techniques, showcasing the potential efficacy of prompts optimization which expands the zero-shot capability of foundation models like SAM.

References

- David Acuna, Huan Ling, Amlan Kar, and Sanja Fidler. Efficient interactive annotation of segmentation datasets with Polygon-RNN++. In *CVPR*, 2018.
- Yuri Y Boykov and M-P Jolly. Interactive graph cuts for optimal boundary & region segmentation of objects in nd images. In *ICCV*, 2001.
- Hu Cao, Yueyue Wang, Joy Chen, Dongsheng Jiang, Xiaopeng Zhang, Qi Tian, and Manning Wang. Swin-UNET: UNet-like pure transformer for medical image segmentation. In *ECCV Workshops Computer Vision*, 2023.
- Lluis Castrejon, Kaustav Kundu, Raquel Urtasun, and Sanja Fidler. Annotating object instances with a Polygon-RNN. In *CVPR*, 2017.
- Dongjie Cheng, Ziyuan Qin, Zekun Jiang, Shaoting Zhang, Qicheng Lao, and Kang Li. Sam on medical images: A comprehensive study on three prompt modes. *arXiv preprint arXiv:2305.00035*, 2023.
- Antonio Criminisi, Toby Sharp, and Andrew Blake. GeoS: Geodesic image segmentation. In *ECCV*, 2008.
- Ruining Deng, Can Cui, Quan Liu, Tianyuan Yao, Lucas W Remedios, Shunxing Bao, Bennett A Landman, Lee E Wheless, Lori A Coburn, Keith T Wilson, et al. Segment anything model (SAM) for digital pathology: Assess zero-shot segmentation on whole slide imaging. *arXiv preprint arXiv:2304.04155*, 2023.
- Lee R Dice. Measures of the amount of ecologic association between species. *Ecology*, 26(3): 297–302, 1945.
- Leo Grady. Random Walks for Image Segmentation. *IEEE Transactions on Pattern Analysis and Machine Intelligence*, 28(11):1768–1783, 2006.
- Sheng He, Rina Bao, Jingpeng Li, P Ellen Grant, and Yangming Ou. Accuracy of segment-anything model (SAM) in medical image segmentation tasks. *arXiv preprint arXiv:2304.09324*, 2023.
- Mohammad Hesam Hesamian, Wenjing Jia, Xiangjian He, and Paul Kennedy. Deep learning techniques for medical image segmentation: achievements and challenges. *Journal of Digital Imaging*, 32:582–596, 2019.
- Yuhao Huang, Xin Yang, Lian Liu, Han Zhou, Ao Chang, Xinrui Zhou, Rusi Chen, Junxuan Yu, Jiongquan Chen, Chaoyu Chen, et al. Segment anything model for medical images? *arXiv preprint arXiv:2304.14660*, 2023.
- Fabian Isensee, Paul F Jaeger, Simon AA Kohl, Jens Petersen, and Klaus H Maier-Hein. nnU-Net: a self-configuring method for deep learning-based biomedical image segmentation. *Nature Methods*, 18(2):203–211, 2021.

- Ge-Peng Ji, Deng-Ping Fan, Peng Xu, Ming-Ming Cheng, Bowen Zhou, and Luc Van Gool. SAM struggles in concealed scenes – empirical study on “segment anything”. *arXiv preprint arXiv:2304.06022*, 2023a.
- Wei Ji, Jingjing Li, Qi Bi, Wenbo Li, and Li Cheng. Segment anything is not always perfect: An investigation of SAM on different real-world applications. *arXiv preprint arXiv:2304.05750*, 2023b.
- Alexander Kirillov, Eric Mintun, Nikhila Ravi, Hanzi Mao, Chloe Rolland, Laura Gustafson, Tete Xiao, Spencer Whitehead, Alexander C. Berg, Wan-Yen Lo, Piotr Dollár, and Ross Girshick. Segment anything. *arXiv:2304.02643*, 2023.
- Wenhao Li, Qisen Xu, Chuyun Shen, Bin Hu, Fengping Zhu, Yuxin Li, Bo Jin, and Xiangfeng Wang. Interactive medical image segmentation with self-adaptive confidence calibration. *arXiv preprint arXiv:2111.07716*, 2021.
- Xuan Liao, Wenhao Li, Qisen Xu, Xiangfeng Wang, Bo Jin, Xiaoyun Zhang, Yanfeng Wang, and Ya Zhang. Iteratively-refined interactive 3d medical image segmentation with multi-agent reinforcement learning. In *CVPR*, 2020.
- Di Lin, Jifeng Dai, Jiaya Jia, Kaiming He, and Jian Sun. ScribbleSup: Scribble-supervised convolutional networks for semantic segmentation. In *CVPR*, 2016.
- Yihao Liu, Jiaming Zhang, Zhangcong She, Amir Kheradmand, and Mehran Armand. SAMM (segment any medical model): A 3D slicer integration to SAM. *arXiv preprint arXiv:2304.05622*, 2023.
- Chaofan Ma, Qisen Xu, Xiangfeng Wang, Bo Jin, Xiaoyun Zhang, Yanfeng Wang, and Ya Zhang. Boundary-aware supervoxel-level iteratively refined interactive 3d image segmentation with multi-agent reinforcement learning. *IEEE Transactions on Medical Imaging*, 40(10):2563–2574, 2021.
- Jun Ma and Bo Wang. Segment anything in medical images. *arXiv preprint arXiv:2304.12306*, 2023.
- Christian Mattjie, Luis Vinicius de Moura, Rafaela Cappelari Ravazio, Lucas Silveira Kupssinskü, Otávio Parraga, Marcelo Mussi Delucis, and Rodrigo Coelho Barros. Exploring the zero-shot capabilities of the segment anything model (sam) in 2d medical imaging: A comprehensive evaluation and practical guideline. *arXiv preprint arXiv:2305.00109*, 2023.
- Maciej A Mazurowski, Haoyu Dong, Hanxue Gu, Jichen Yang, Nicholas Konz, and Yixin Zhang. Segment anything model for medical image analysis: an experimental study. *arXiv preprint arXiv:2304.10517*, 2023.
- Volodymyr Mnih, Koray Kavukcuoglu, David Silver, Alex Graves, Ioannis Antonoglou, Daan Wierstra, and Martin Riedmiller. Playing atari with deep reinforcement learning. *arXiv preprint arXiv:1312.5602*, 2013.

- Volodymyr Mnih, Koray Kavukcuoglu, David Silver, Andrei A Rusu, Joel Veness, Marc G Bellemare, Alex Graves, Martin Riedmiller, Andreas K Fidjeland, Georg Ostrovski, et al. Human-level control through deep reinforcement learning. *Nature*, 518(7540):529–533, 2015.
- Sovesh Mohapatra, Advait Gosai, and Gottfried Schlaug. Brain extraction comparing segment anything model (SAM) and fsl brain extraction tool. *arXiv preprint arXiv:2304.04738*, 2023.
- Long Ouyang, Jeffrey Wu, Xu Jiang, Diogo Almeida, Carroll Wainwright, Pamela Mishkin, Chong Zhang, Sandhini Agarwal, Katarina Slama, Alex Ray, et al. Training language models to follow instructions with human feedback. In *NeurIPS*, 2022.
- Martin Rajchl, Matthew CH Lee, Ozan Oktay, Konstantinos Kamnitsas, Jonathan Passerat-Palmbach, Wenjia Bai, Mellisa Damodaram, Mary A Rutherford, Joseph V Hajnal, Bernhard Kainz, et al. DeepCut: Object segmentation from bounding box annotations using convolutional neural networks. *IEEE Transactions on Medical Imaging*, 36(2):674–683, 2016.
- Olaf Ronneberger, Philipp Fischer, and Thomas Brox. U-Net: Convolutional networks for biomedical image segmentation. In *MICCAI*, 2015.
- Carsten Rother, Vladimir Kolmogorov, and Andrew Blake. GrabCut: interactive foreground extraction using iterated graph cuts. *ACM Transactions on Graphics*, 23(3):309–314, 2004.
- Saikat Roy, Tassilo Wald, Gregor Koehler, Maximilian R Rokuss, Nico Disch, Julius Holzschuh, David Zimmerer, and Klaus H Maier-Hein. SAM.MD: Zero-shot medical image segmentation capabilities of the segment anything model. *arXiv preprint arXiv:2304.05396*, 2023.
- Neeraj Sharma and Lalit M Aggarwal. Automated medical image segmentation techniques. *Journal of Medical Physics*, 35(1):3, 2010.
- Gwangmo Song, Heesoo Myeong, and Kyoung Mu Lee. SeedNet: Automatic seed generation with deep reinforcement learning for robust interactive segmentation. In *CVPR*, 2018.
- Richard S Sutton and Andrew G Barto. *Reinforcement learning: An introduction*. MIT press, 2018.
- Guotai Wang, Maria A Zuluaga, Wenqi Li, Rosalind Pratt, Premal A Patel, Michael Aertsen, Tom Doel, Anna L David, Jan Deprest, Sébastien Ourselin, et al. DeepIGeoS: A deep interactive geodesic framework for medical image segmentation. *IEEE Transactions on Pattern Analysis and Machine Intelligence*, 41(7):1559–1572, 2018.
- Christopher JCH Watkins and Peter Dayan. Q-learning. *Machine learning*, 8:279–292, 1992.
- Jason Wei, Yi Tay, Rishi Bommasani, Colin Raffel, Barret Zoph, Sebastian Borgeaud, Dani Yogatama, Maarten Bosma, Denny Zhou, Donald Metzler, Ed H. Chi, Tatsunori Hashimoto, Oriol Vinyals, Percy Liang, Jeff Dean, and William Fedus. Emergent abilities of large language models. *Transactions on Machine Learning Research*, 2022. ISSN 2835-8856.

- Julia Wolleb, Robin Sandkühler, Florentin Bieder, Philippe Valmaggia, and Philippe C Cattin. Diffusion models for implicit image segmentation ensembles. In *MIDL*, 2022.
- Junde Wu, Rao Fu, Huihui Fang, Yuanpei Liu, Zhaowei Wang, Yanwu Xu, Yueming Jin, and Tal Arbel. Medical SAM adapter: Adapting segment anything model for medical image segmentation. *arXiv preprint arXiv:2304.12620*, 2023.
- Ning Xu, Brian Price, Scott Cohen, Jimei Yang, and Thomas S Huang. Deep Interactive Object Selection. In *CVPR*, 2016.
- Chunhui Zhang, Li Liu, Yawen Cui, Guanjie Huang, Weilin Lin, Yiqian Yang, and Yuehong Hu. A comprehensive survey on segment anything model for vision and beyond. *arXiv preprint arXiv:2305.08196*, 2023.
- Kaidong Zhang and Dong Liu. Customized segment anything model for medical image segmentation. *arXiv preprint arXiv:2304.13785*, 2023.
- Yichi Zhang and Rushi Jiao. How segment anything model (SAM) boost medical image segmentation? *arXiv preprint arXiv:2305.03678*, 2023.
- Feng Zhao and Xianghua Xie. An overview of interactive medical image segmentation. *Annals of the BMVA*, 2013(7):1–22, 2013.
- Hong-Yu Zhou, Jiansen Guo, Yinghao Zhang, Lequan Yu, Liansheng Wang, and Yizhou Yu. nnFormer: Interleaved transformer for volumetric segmentation. *arXiv preprint arXiv:2109.03201*, 2021.
- Tao Zhou, Yizhe Zhang, Yi Zhou, Ye Wu, and Chen Gong. Can SAM segment polyps? *arXiv preprint arXiv:2304.07583*, 2023.